JOURNAL OF MATERIALS SCIENCE **39** (2004) 7041–7047

Phase transformations and structure characterization of calcium polyphosphate during sintering process

LINGHONG GUO*, HUI LI
PANalytical XRD Application Research Laboratory, Analysis and Testing Center, Sichuan University, Chengdu 610065, People's Republic of China
E-mail: guolinghong@sohu.com

XIAHONG GAO
College of Chemical Engineering, Sichuan University, Chengdu 610065, People's Republic of China

Calcium polyphosphate (CPP) may be a promising bone substitute with controllably degraded ability. In this investigation, the effects of sintering temperatures on CPP's phase transformations and microstructure parameters, such as the distribution of crystallite size and micro-strain, were investigated by X-ray diffraction (XRD). The qualitative phase analysis and quantitative phase analysis based on reference intensity ratio (RIR) method were conducted for the CPP sintered at 585, 600, 650, 700, 750, 800 and 900°C. The distribution of crystallite size and micro-strain were calculated with the Warren-Averbach Fourier Transfer method. The results demonstrated that the transformation of amorphous CPP to semi-crystalline CPP occurred below 585°C, and semi-crystalline CPP to γ-CPP at temperature of 585–600°C; γ-CPP to β-CPP at 585–700°C. CPP sintered between 600–700°C were composed of both γ-CPP and β-CPP, and the mass fraction of β-CPP increased with rising of temperature. Above 700°C, the sintered CPP only contained β-CPP. At different ranges of the sintering temperature, the average crystallite size (D) and micro-strain (ε) showed significant difference, for example, D and ε is about 2.9 nm and 1.68% at 585°C, but D and ε was 8.0 to 8.7 nm and 0.159 to 0.134% at 600 and 700°C, respectively. The results of the phase transformations and the variations of microstructure parameters in the present study may be able to provide some fundamental data for explaining CPP degradation phenomena.

1. Introduction

Being similar in chemical composition and structure to biological bone, calcium phosphates have demonstrated excellent biocompatibility and the ability to form a continuous interface with bone. The emergence of calcium phosphates has expanded the selection of bone substitutes for restorative and substitutive osteoplastic surgery. These man-made bone substitutes avoid a series of problems related to the use of autografts and allografts, such as, surgerical morbidity, blood loss, and inherent immunogenicity. The specific calcium phosphates used as bone substitutes are tri-calcium phosphate (β-TCP) and hydroxyapatite (HAP). Although HAP and β-TCP have been used as bone substitutes for decades, the brittleness of HAP and β-TCP, and the non-degradability of HAP and the unacceptable degradability of β-TCP have greatly limited their further clinical application [1, 2].

The search for new kind of calcium phosphates with suitable biodegradation rates has attracted many research groups [3–10]. Using a high temperature sintering method, Pilliar [4] and Kim [5] developed calcium polyphosphate or calcium meta-phosphate (CPP, $[Ca(PO_3)_2]n$). Sinyaev [6] synthesized amorphous CPP in solution by mixing the solution of sodium polyphosphate with calcium chloride. Casting and rapid prototype technologies, such as sterolithography, have been used to fabricate the dense CPP ceramics with compressive strengths over 280 MPa which were suitable for use as tooth crowns and bone screws [8, 9]. Porous CPP ceramics have demonstrated better mechanical properties than porous HAP ceramics with same porosity [10].

A great number of experiments *in vivo* and *in vitro* have proved that CPP is biocompatible and bioactive [4, 11–15]. *In vivo* and *in vitro*, the porous and dense CPP ceramics showed biodegradation rates which varied significantly [7, 8, 12, 13, 16, 17]. *In vivo* CPP fibers

*Author to whom all correspondence should be addressed.

degraded totally within 16 weeks in rat muscle, and within 20 weeks after implantation in Achilles tendons and subcutaneous layers of rats according to X-ray and pathological examination [15]. *In vitro*, porous CPP ceramics sintered at different temperatures (585–900°C) also demonstrated greatly different degradation rates *in vitro*. For example, 24.19% of total phosphorus in CPP sintered at 585°C was degraded after 5 day of immersion in 0.1 M tris-buffered solution, but only 2.72% of total phosphorus in CPP sintered at 600°C was degraded after 10 days in same solution [10]. Assuming that the degradation rate of CPP is proportional to the immersion time, CPP sintered at 585°C will degrade completely in 6.5 days, which is 17.8 faster than CPP sintered at 600°C. Dense CPP ceramics cast or sintered at higher temperature do not biodegrade totally [8, 9].

The variation in the degradation rates leads to the idea that it might be possible to control the biodegradability of CPP, such that degradation rate of CPP could be tailored in order to meet clinical requirements for bone substitutes with different degradation rates. Unfortunately, there is presently no report of the variation of degradation with CPP crystal structure. Some apparent factors, such as the size of CPP starting particles or sintering temperatures, were attributed to this variation. However phase transformations during sintering process and inherent structure/microstructure parameters were not attributed. The lack of structure study not only probably inhibits the research and development of controllably degraded CPP bone substitutes, but also further inhibits the understanding of the mechanism of CPP degradation *in vivo*.

CPP is an inorganic polymer whose crystal structure which includes γ-CPP, β-CPP, α-CPP, is very complex. It has reported that γ-CPP will transfer to β-CPP at temperature of 500–700°C, and α-CPP will be formed from the transformation of β-CPP at 985°C [18]. With respect to the condensed state structure, there are three kinds of net structure of $[Ca(PO_3)_2]n$: linear chain structure, ring chain structure, and three-dimension cage structure.

Because of the CPP being multiphase, the phase composition of CPP ceramics should be an important factor in controlling the CPP degradation rate. Other microstructure parameters, such as, crystallite size and micro-strain, may be also play a certain role in the CPP degradation phenomena.

The objectives of this study were to investigate the effects of sintering temperature on the phase transformations, and to investigate the distribution of the crystallite size and average micro-strain. The phase transformations of CPP during the sintering process, which went up to 900°C were investigated by X-ray diffraction (XRD). The distribution of crystallite sizes/average crystallite size and micro-strain, were also calculated by the Warren-Averbach Fourier Transfer (W-A/FT) method [16, 19].

2. Materials and methods

Chemical grade $Ca(H_2PO_4)_2{\cdot}H_2O$ was placed into a 500 ml Al_2O_3 crucible with high purity ($Al_2O_3\% >$ 99), and was calcined at 500°C for 10 h in atmosphere through the following polymerization reaction [10]:

$$n\mathrm{Ca(H_2PO_4)_2 \cdot H_2O} = [\mathrm{Ca(PO_3)_2}]n + 3n\mathrm{H_2O}$$

The calcined aggregate with crucible was melted at 1150°C for 2 h and the molten CPP was poured into distilled water in order to produce glass-like CPP particles with the diameters less then 10 mm. These glass-like CPP particles were put into a ball milling and ground for 24 h in order to obtain the fine powders, the ground CPP powders was sieved by 200 meshes for further sintering experiments.

The prepared glass-like powders were sintered in an electric oven at temperatures of 585, 600, 650, 700, 750, 800 and 900°C, respectively. The rate of rising temperature was 5°C/min and it dwelled at the set sintering temperature for two hours, then the power was turn off and the sintered samples were remained in the oven for cooling in the atmosphere. The oven was controlled by the program and the fluctuation of the sintering temperature was around the set temperature of less then $1^\circ(\pm<1^\circ)$.

The sintered CPP powders were then analyzed for XRD experiments preformed on the X'Pert Pro MPD X-ray diffractometer (Philips, Netherlands). The voltage and anode current were 40 KV and 40 mA, respectively. The Cu $K_\alpha = 0.15405$ nm and continuous scanning mode with 0.02 step size and 0.5 s of set time were used in all XRD experiments for collecting the data of samples. Further, in order to increase the intensity the parallel X-ray incident beams was the hybrid mirror with a divergence slit of 1/16° and a sollar slit of 0.04 Rad; for the diffracted beam the parallel plate collimator with a sollar slit 0.04 Rad and the prepositional detector were used in all XRD experiments.

The qualitative phase analysis was performed with X'Pert HighScore software package (Philips, Netherlands) and PDF2-2003 database (International Center for Diffraction Data, PA, USA). The usage of X'Pert HighScore gives the dynamic match and obvious marks for matched and unmatched reflections. Thus the qualitative phase analysis can be easily completed for the multiphase mixture with the overlapping reflections. This is especially useful for identifying the phases from the XRD pattern of the CPP system because the reflections of α-CPP, β-CPP, γ-CPP, overlap each other.

The quantitative phase analysis in X'Pert HighScore works on basis of the RIR (Reference Intensity Ratio) values. These values are often called I/I_c values. The definition of RIR value is on the relative net peak height ratio of the strongest line ($I_{rel} = 100\%$) of the phase and the strongest line of corundum, measured with Cu K_α radiation in a mixture of equal weight percentages. The set of RIR values published in PDF2-2003 was measured or calculated by several famous XRD laboratories in the world. RIR method determines the mass fractions of the identified phases in a mixture system [17, 20–22]. The mass fraction X_α of phase α in the mixture is calculated from Equation 1:

$$X_\alpha = [I_\alpha/\mathrm{RIR}_\alpha] \times \left[\sum I_i/\mathrm{RIR}_i\right] \qquad (1)$$

RIR_i is the reference intensity ratio of the ith phase of the mixture, and I_i is the intensity of the strongest peak of the ith phase in the analyzed mixture. During the quantitative phase analysis of the X'Pert HighScore, I_i and RIR_i are obtained automatically from the PDF2-2003 database.

The breading of reflections in XRD pattern is attributed to the contributions of crystallite size, micro-strain (ε), and the instrument itself. The experimental profile function $h\ (\theta)$ of the reflection was convoluted by the profile functions of the distribution of crystallite size $g\ (\theta)$ and micro-strain $fn\ (\theta)$, as well as the instrumental profile function $fm\ (\theta)$

$$h(\theta) = g(\theta) \oplus fn(\theta) \oplus fm(\theta) = \int_{-\infty}^{+\infty} \int_{-\infty}^{+\infty} g(y) fn(\zeta) fm(\theta - (y - \zeta))\, \mathrm{d}\zeta\ dy \tag{2}$$

In order to obtain the distribution of crystallite size and average micro-strain, the experimental profile function $h(\theta)$ of broadening reflections must be deconvoluted. The scan of the standard samples without micro-strain and crystallite size greater than 200 nm will define the instrumental broadening of reflections in the standard sample's XRD pattern.

The objective of profile analysis is to separate the effects of the crystallite size and micro-strain on reflection broadening based on the instrumental profile function $fm(\theta)$. Fourier-transfer deconvolution is able to analyze the profile of broadening reflections and separate the effects of crystallite size (3 nm $< D <$ 200 nm) and micro-strain on broadening reflections. Introduced by Warren and Averbach in 1950's, Fourier-transfer deconvolution method has not been widely used because the mathematical process is cumbersome [23].

In the present study, the software based on the Warren-Averbach Fourier Transfer (W–A/FT) method was used to calculate the distribution of crystallite size and micro-strain of the sintered CPP. The polycrystalline silicon supplied by the Philips Company was used as the standard without the reflection broadening of crystalline size (>200 nm) and micro-strain (annealed), and measured with the same instrumental conditions as CPP. The broadening reflections at 2θ range of 26.5 to 28.2° for crystalline CPP and the significantly broadening reflections at 2θ range of 20–30° for glass-like CPP and semi-crystalline CPP were calculated with the W-A/FT method.

3. Results and discussion

Hench [24] postulated the definition of the 3rd generation of biomaterials, both bioactive and biodegradable materials. When viewing materials science, searching and developing the controllably biodegradable scaffold is one of the main tasks for biomaterials science and engineering. The precursors of CPP are either calcium hydrogen phosphates or other calcium acid-phosphates with the Ca/P atom ratio of 0.5. Comparing these to calcium base-phosphates with the higher Ca/P ratio, such as 1.5 of TCP or 1.67 of HAP, the higher dissolution of the precursors makes it possible for CPP to be completely degraded *in vivo* and *in vitro*. On the other hand, the variation in the polymerization degree of CPP, an inorganic polymer, makes it degrade with the adjustable rates.

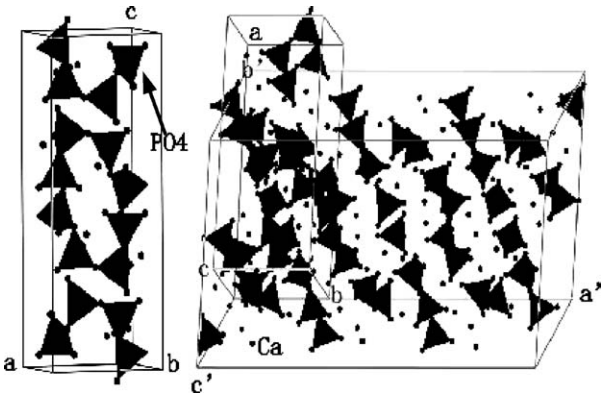

Figure 1 3-D structureds of CPP (left) and Calcium meta-phosphate (right). (Tetrahedron: PO_4; P atom locate in the center of tetrahedrons, free black points: Ca atom. In Fig. 1b (right), abc: the primary cell; $a'b'c'$: the complex cell.)

In vivo implantation experiments, porous CPP ceramics is osteoconductive and promotes rapid bone growth. It can be tailored to degrade at a given rate through appropriate selection of sintering temperatures or the starting particle sizes [6, 9]. Except for *in vitro* and *in vivo* implantation, basic research about CPP structures is urgently needed for adjusting its biodegradation rate and tailoring its other properties.

Fig. 1a and b show the 3-D crystal structures of β-CPP (1a) and calcium meta-phosphate (1b). β-CPP crystal structure was constructed based on the following data [25]: monoclinic system; space group: P21/c; lattice parameter: $a = 0.69600$ nm; $b = 0.77114$ nm; $c = 1.6994$ nm; $\alpha(^\circ) = 90.0000$; $\beta(^\circ) = 90.4400$; $\gamma(^\circ) = 90.0000$. The crystal cell of β-CPP is composed of two elemental units consisting of a circular chain connected by eight PO_4 tetrahedrons. The polymerization of $[Ca(PO_3)_2]$ probably results in the connection of two circle chain units through O atoms at the two circle chains. The β-CPP polymerization will produce a complex chain structure along the C axis which will probably result in the small change of crystal cell dimensions and the coordinate of Ca atoms in the cell. From the above analysis, the different polymerization degrees of CPP sintered at different temperatures will have the same space group and crystal system. But it will be different in the cell dimensions and reflection intensities in the XRD pattern.

Unfortunately, there is no available γ-CPP structure in ICSD database. There is another kind of $[Ca(PO_3)_2]n$, calcium meta-phosphate with monoclinic system (Space group: P21/a; lattice parameter: $a = 1.69600$ nm; $b = 0.77144$ nm; $c = 0.69963$ nm ; $\alpha(^\circ) = 90.0000$; $\beta(^\circ) = 90.3940$; $\gamma(^\circ) = 90.0000$)) [23]. The crystal cell of calcium meta-phosphate is similar with β-CPP in many features, such as, cell dimensions, and cell volume *etal*. The obvious and significant difference is that the crystal cell of calcium meta-phosphate

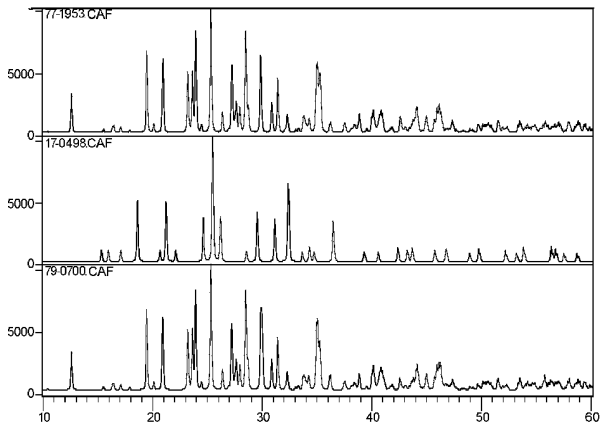

Figure 2 Standard XRD patterns of β-CPP (top), γ-CPP (middle) and calcium meta-phosphate (bottom).

is composed of the elemental units which are simple liner chains connected by two PO_4 tetrahedrons. Therefore, this kind of compound is named calcium meta-phosphate. It is a meta-state. Calcium meta-phosphate may be the precursor of β-CPP in the sintering process.

In the powder diffraction files (PDF2-2003 Version), there are XRD patterns of β-CPP (PDF 77-1953), γ-CPP (PDF 17-498) and calcium meta-phosphate (PDF 79-700). Fig. 2 demonstrates the calculated XRD patterns of β-CPP (PDF 77-1793) and calcium meta-phosphate (PDF 79-700), as well as the experimental XRD pattern of γ-CPP (PDF 17-489). There are many reflections on each XRD pattern. The positions of stronger reflections in each pattern are almost at the same 2θ position. The phase analysis of the CPP system will meet great difficulty, which may have result in lack of XRD patterns shown in previous references [3–6, 10].

The Figs 3–5 shows the XRD patterns of the glass-like CPP powders and semi-crystalline or crystalline CPP powders sintered at different temperatures. The symmetrical diffuse reflection around $2\theta = 25^\circ$ in Fig. 3 indicated that the prepared starting CPP powders was typical amorphous. For CPP sintered at 585°C, the original symmetrical diffuse reflection began to spilt

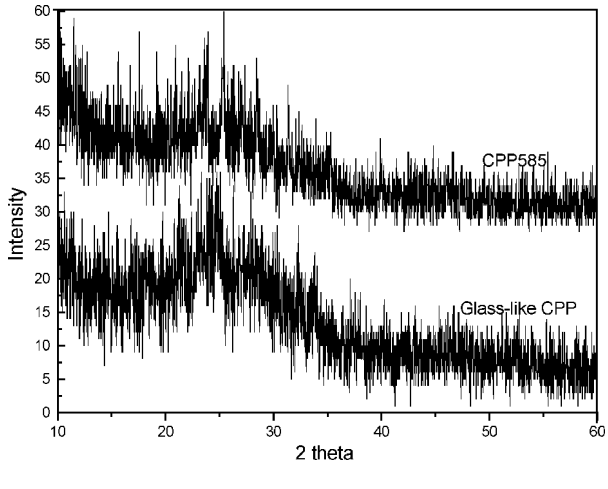

Figure 3 XRD patterns of the glass-like CPP and semi-crystalline CPP (CPP585).

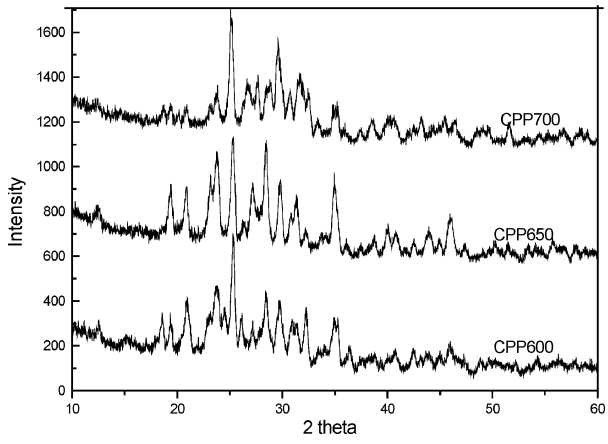

Figure 4 XRD patterns of the crystalline CPP sintered at 600°C (CPP600), 650°C (CPP650), 700°C (CPP700).

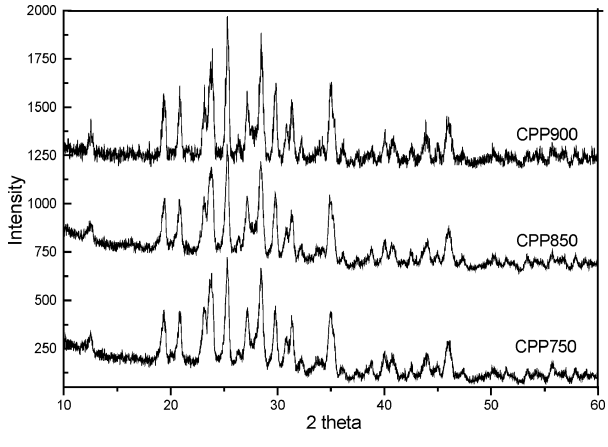

Figure 5 XRD patterns of the crystalline β-CPP sintered at 750°C (CPP750), 800°C (CPP800), 900°C (CPP900).

into two symmetrical diffuse reflections, which indicated that at that phase transformation began at or below 585°C. Its diffuse characteristic of these two reflections was very difficult to identify the phase and the occurrence of this transformation before crystallizing. So the CPP sintered at 585°C was named semi-crystalline CPP in the present study.

Compared with XRD patterns of CPP585 and CPP600, the transformation of semi-crystalline CPP to crystalline CPP occurred at the narrow temperature range of 585–600°C. In this stage, the transformation of γ-CPP to β-CPP also occurred. The presence of β-CPP in this stage illustrated that: (1) The γ-CPP is unstable and it exists at a very narrow temperature range ($585 < T < 600$°C); (2) The crystallization rate of semi-crystalline CPP to crystalline CPP was faster than that of γ-CPP to β-CPP.

Fig. 4 demonstrates the XRD patterns of CPP sintered at 600, 650 and 700°C. The intensity of the reflections in 2θ range of 26.5° to 28.2° increased with the rising of the sintering temperature. The variation of the relative intensity on XRD patterns indicates that the sintered CPP contained more than one phase including β-CPP and that the mass fraction of β-CPP in sintered CPP increased. McIntosh [18] reported that the transformation of γ-CPP to β-CPP occurred at 500–700°C. Filiaggi [26] reported that there was only β-CPP in the

TABLE I Phase composition of the sintered CPP calculated with RIR method

Mass fraction	CPP600[a]	CPP650	CPP700	CPP750	CPP800	CPP900
γ-CPP (%)	41	39	32	0	0	0
β-CPP (%)	59	61	68	100	100	100

[a]In term of CPPxxx, xxx was sintering temperature.

CPP ceramics sintered above 600°C. The transformation of γ-CPP to β-CPP occurred at 600–700°C, and the mass fraction of β-CPP depended on the dynamics of the transformation determined by the sintering temperatures and the rate of rising temperature. Fig. 5 illustrates the XRD patterns of CPP sintered at 750, 800 and 900°C, respectively. There were no obvious differences in position and relative intensity of each reflection for CPP sintered above 700°C. The CPP sintered above 750°C was composed of only β-CPP, and there was no detectable γ-CPP for the limitation ($<1\%$) of XRD qualitative phase analysis.

Table I lists the quantitative analysis of the sintered CPP at different temperatures. The RIR values of β-CPP and calcium meta-phosphate are 0.580 and 0.585 from the PDF2 database. Unfortunately, the RIR and parameters of crystal structure of γ-CPP is not available. From the above discussion about crystal structures of β-CPP and calcium meta-phosphate, calcium meta-phosphate may be the precursor of β-CPP. In the present study, the results of phase transformation verified that γ-CPP was the precursor of β-CPP. On the other hand, γ-CPP and β-CPP, and calcium meta-phosphate have the same chemical formula $[Ca(PO_3)_2]n$, and a similar crystal structure. Assumption of RIR 0.585 of calcium meta-phosphate same as γ-CPP's RIR, 0.585, was reasonable. From the error analysis of $\Delta X_\alpha / X_\alpha$ relation with RIR_α and ΔRIR_α for Equation 1, this assumption would not produce the significant error for the results of quantitative analysis. During the practical quantitative analysis of X'Pert HighScore, the mass fraction of γ-CPP in CPP700 changed from 32 to 34% accompanying the RIR of γ-CPP 0.585 replaced by 0.580.

Theoretically RIR quantitative analysis method should give the exact results of the mass fraction of a mixture. Practically speaking, however, several sources of errors maybe prohibit an accurate result. The main errors are: (1) The RIR values from the reference database: In the present study, the assumption of RIR of γ-CPP being equal to calcium meta-phosphate RIR (0.585) might result in a certain error theoretically. (2) The overlapping of the strongest reflection will result in the wrong intensity for each phase. In order to obtain the intensity of β-CPP and γ-CPP, the deconvolution of overlapping diffraction lines was processed with a profile-fit based Voigt function constructed in the X'Pert HighScore.

Except for the phase composition, the distribution of crystallite size and average microstrain are also the important parameters for characterizing microstructure [27]. Fig. 6 plots the average micro-strains and average crystallite sizes vs. sintering temperatures. The software based on the W-A/FT method outputs the distribution of crystallite size and average crystallite size, as well as average micro-stain. The distribution of crystallite size, a graph (not shown in the present study), is difficult to plot with variation of the sintering temperatures. To easily compare the effects of sintering, the values of average crystallite size and average micro-strain were plotted with the sintering temperatures. The increase of the average crystallite size corresponded to the decrease of average micro-strain with increasing sintering temperature at each sintering stage. Both tendencies of increase and decrease at the same temperature range were very similar, indicating that two microstructure parameters might be closely correlated together.

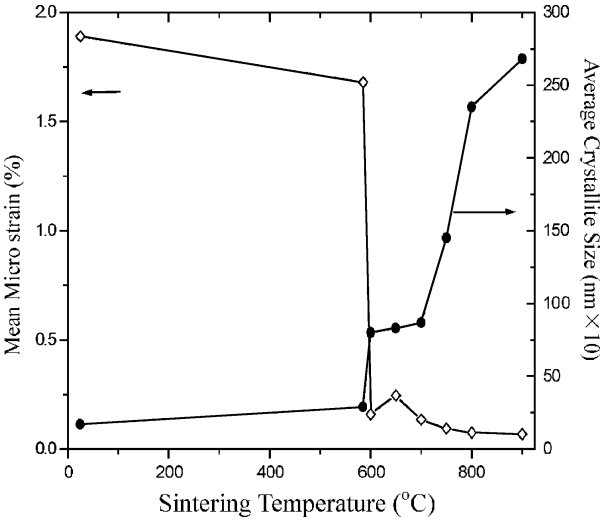

Figure 6 Average crystallite size and mean micro-strain of sintered CPP vs. sintering temperatures.

The Scherrer equation is widely used to calculate average crystallite size, but this method uses only the strongest diffraction and neglects the contribution of micro-strain for broadening of reflections. By means of Scherrer equation, the average crystallite sizes calculated from different reflections are often significantly different from each other because of the contribution of micro-strain to broadening of the reflections. In order to obtain the actual value of average crystallite size, the effect of crystallite size and micro-strain on reflection broadening should be separated.

We found that when comparing with the glass-like CPP and semi-crystalline CPP sintered at 585°C, below 585°C the average crystallite size increased slightly but the micro-strain decreased to some degree as well. The main feature of this sintering stage was the perfecting of crystalline structure, that is, the increase of the crystallite size and decrease of the micro-strain.

At the sintering temperatures between 585–600°C, it was observed that both phase transformations from semi-crystalline to γ-CPP and γ-CPP to β-CPP occurred. The average crystallite size abruptly increased from 2.9 nm of semi-crystalline to 8.0 nm of β-CPP and micro-strain decreased significantly at the same time. Two kind of the phase transformations and further perfecting of crystals were the characteristics of the sintering process between 585–600°C. In the range

of 600–700°C, the growth of CPP crystals seemed to cease temporarily, and CPP crystals only grew from 8.0 to 8.9 nm, and micro-strain decreased slightly from 0.159 to 0.134%. The phase transformation from γ-CPP to β-CPP occurred, and the β-CPP/γ-CPP weight ratio increased with rising of sintering temperature. The obvious characteristic of sintering process at this stage was the phase transformation form γ-CPP to β-CPP.

Abe [28] reported that the crystallization of amorphous CPP took place at 600–660°C. In the present experiments, the crystallization temperature was below 600°C, and the process of crystallization mainly occurred at 585–600°C. Above 700°C, the transformation of γ-CPP to β-CPP was completed. With the rising of the sintering temperature, the crystallite size of β-CPP increased steadily and micro-strain further decreased. The main change occurring in this temperature range was the perfecting of β-CPP crystal lattice.

The effects of sintering temperature on CPP crystalline structure are very complex, involving thermodynamics and dynamics of the transformations. In the present study, the sintering process can be marked as several stages. At below 585°C and above 700°C, the average crystallite size and micro-strain might be used to characterize the crystal growth and perfecting of semi-crystalline or crystalline phase. In the narrow range of temperature between 585 to 600°C, two kinds of transformations occurred. In the range of 600–700°C, the transformation of γ-CPP to β-CPP was featured by the mass fraction increase of β-CPP, and the perfecting of crystal by increase of the average crystallite size and decrease of micro-strain. For explaining CPP degradation *in vivo* and *in vitro*, the correlation of above micro-structural parameters' change with the variation of degradation rates might be more reasonable than the porosity of CPP ceramics or sintering temperatures.

The phase composition of CPP ceramics is very crucial for its degradation rate *in vivo*. The phase transformation of CPP during sintering process is very important for understanding the degradation phenomena of CPP. During the sintering processes up to 900°C, three kinds of main phase transformation occurred, that is, amorphous CPP to semi-crystalline CPP, semi-crystalline CPP to γ-CPP, and γ-CPP to β-CPP. Comparing with the degradation data of CPP, the former phase transformation is a key factor for adjusting the degradation rate because the degradation rate of CPP585 is about 18 times faster than CPP600 [10]. The degradation rates of the porous CPP ceramics sintered above 600°C did not demonstrate significant differences, which probably attributed to similar properties between β-CPP and γ-CPP. In order to be able to characterize glass-like or semi-crystalline and crystalline, the distribution of crystallite size/mean crystalline size and micro-strain may be the only available microstructure parameters because of difficulty in characterization of the amorphous or semi-crystals in structural terms.

Combined with the phase transformations occurring at 585–600°C, the great difference of 2.7 and 8.0 nm in average crystallite size and 1.68 and 0.159% in micro-strain for both CPP585 and CPP600 satisfactorily explained their significant difference in the degradation rates *in vitro* and *in vivo*.

The future work of this investigation will focus on (1) using radical distribution function (RDF) to characterize amorphous CPP and semi-crystalline CPP; (2) with the help of the Molecular Simulation Workstation (Cerius^2, MSI Company, USA), constructing the chain structure with different polymerization degrees base on the crystal cells of β-CPP and calcium meta-phosphate, and simulating and computing the XRD patterns, and compare with experimental XRD patterns.

4. Conclusions

The present study confirmed that during the sintering process for fabricating CPP ceramics there is a series of phase transformations with XRD qualitative analysis and quantitative analysis. The results demonstrate that the sintering temperature significantly influenced CPP's phase transformations and microstructure parameters.

During the sintering process from room temperature to 900°C, the transformations of semi-crystalline CPP to crystalline CPP, that is, crystallization process, mainly occurred within a narrow temperature range of 585–600°C. The transformation of γ-CPP to β-CPP occurred at two sintering temperature ranges of 585 to 600°C and 600 to 700°C. In term of the perfecting of the CPP crystallizing process characterized with average crystallite size (D) and micro-strain (ε), D increased and ε decreased with rising of the sintering temperature. The perfecting process mainly occurred around 600°C and above 700°C.

The phase transformations of CPP during the sintering process and the characteristics of CPP microstructure provide the fundamental data for developing controllable-degraded CPP bioceramics.

References

1. W. SUCHANEK and M. YOSHIMURA, *J. Mater. Res.* **13** (1998) 94.
2. S. D. BODEN, *Tissue Eng.* **6** (2000) 383.
3. D. BAKSH and J. E. DAVIES, *J. Mater. Sci.: Mater. In Med.* **9** (1999) 743.
4. R. M. PILLIAR, M. J. FILIAGGI, J. D. WELLS, M. D. GRYNPAS and R. A. KANDEL, *Biomaterials* **22** (2001) 963.
5. J. LEE and S. KIM, "Transactions of 5th World Biomaterials Congress," Toronto, Canada, 1996, p. 53.
6. V. A. SINYAEV, E. S. SHUSTIKOVA, L. V. LEVCHENKO and A. A. SEDUNOV, *Inorg. Mater.* **37** (2002) 735.
7. Y. ABE and T. KASUGA, *J. Amer. Ceram. Soc.* **65** (1982) 189.
8. J. W. BARLOW, G. H. LEE, C. R. HRAWFORD, J. J BEAMAN, H. L. MARCUS and R. J. LAGOS, U.S. Patent No. 5,639,402, June 17, 1997.
9. J. W. BARLOW, G. LEE, R. H. CRAWFORD, J. J. BEAMAN, H. L. MARCUS and R. J. LAGOW, US Patent, US 6183515B, Feb. 6, 2001.
10. N. L. PORTER, R. M. PILLIAR and M. D. GRYNPAS, *J. Biomed. Mater. Res.* **56** (2001) 504.
11. S. R. NELSON, L. M. WOLFORD, R. J. LAGOW, P. J. CAPANO and W. L. DAVIS, *J. Oral. Maxillofac. Surg.* **51** (1993) 1363.
12. H. FUKUI, Y. TAKI and Y. ABE, *J. Dent. Res.* **56** (1977) 1260.

13. M. D. GRYNPAS, R. M. PILLIAR, R. A. KANDEL, R. RENLUNS, M. FILIAGGI and M. DUMITRIU, *Biomaterials* **23** (2002) 2063.
14. G. LEE, J. W. BARLOW and W. C. FOX, "Solid Freefrom Fabrication Symposium," edited by H. L. Marcus *et al*. Austin, TX, USA, 1996, p.15.
15. ZHAO LIN and SUN ZHENG-YI, *Chinese J. Reparative and Reconstr. Surg*. **16** (2002) 300.
16. H. TORAYA, *Powder Diffr.* **4** (1989) 70.
17. F. H. CHUNG, *J. Appl. Cryst*. **7** (1974a) 513.
18. A. O. McINTOSH and W. L. JABLONSKI, *Anal. Chem*. **9** (1956) 1424.
19. A. G. LVAREZ and R. D. BONETTO, *Powder Diffraction* **2** (1987) 220.
20. F. H. CHUNG, *J. Appl. Cryst* **7** (1974b) 526.
21. *Idem*., *ibid*. **8** (1975) 17.
22. R. L.SNYDER, *Powder Diffr*. **7** (1992) 186.
23. W. ROTHAMMEL and H BURZLAFF, *Acta Crystallogr.* Sec. C **45** (1989) 551.
24. L. L. HENCH and J. M. POLAK, *Science* **295** (2002) 1014.
25. M. SCHNEIDER, K. H. JOST and P. Z. LEIBNITZ, *Anorg. Allg. Chem*. **99** (1985) 527.
26. M. FILIAGGI, R. PILLIAR and J. HONG, *Key Engng. Mater.,* **192–195** (2001) 171.
27. H. P. KLUG and L. E. ALEXANDER, in "X-ray Diffraction Procedure for Polycrystalline and Amorphous Materials" (John Wiley & Son, 1974).
28. Y. ABE, T. ARAHORI and A. NARUSE, *J. Amer. Ceram. Soc*. **59** (1976) 487.

Received 26 June 2003
and accepted 20 July 2004